Single-Pixel Imaging Using Carrier-Depletion Optical Phased Array With Reduced Phase Shift Requirement

Samar Emara [ORCID], *Student Member, IEEE*, Taichiro Fukui [ORCID], *Student Member, IEEE*, Kento Komatsu [ORCID], Yusuke Kohno, Rui Tang [ORCID], Takuo Tanemura [ORCID], *Member, IEEE*, and Yoshiaki Nakano [ORCID], *Member, IEEE*

Abstract—The optical-phased array (OPA) has gained special interest in recent years as a high-speed and compact imaging device. While large-scale OPAs have been demonstrated in single-pixel imaging, the complexity of the driver circuit is becoming a crucial problem as the number of phase shifters increases. Here, we investigate the phase shift requirement of OPA for single-pixel imaging and demonstrate, for the first time, that full 2π phase shifts are not mandatory to generate a set of illumination patterns with a sufficient degree of randomness required to reconstruct the image. Using a silicon photonic OPA chip with 128 carrier-depletion-based phase shifters, we experimentally confirm this property by successfully retrieving an image under a maximum phase shift of only $\sim 1.5\pi$ without affecting the quality of the image. Consequently, the input voltage can be reduced significantly. Since the carrier-depletion phase shifters generally require high driving voltages, this finding paves the way to high-speed OPA-based imaging with a minimum device requirement.

Index Terms—Optical imaging, optical phased array, photonic integrated circuits, single-pixel imaging.

I. INTRODUCTION

SINGLE-PIXEL imaging has gained growing attention recently [1]–[10] and has been successfully implemented in numerous applications [9], including multi-spectral imaging [10], [11], light-detection-and-ranging (LiDAR) [12]–[14], ophthalmoscope [15], terahertz imaging [16], [17], three-dimensional (3D) imaging [18]–[20], and flow cytometry [21]. By using pseudo-random speckle illumination patterns to image the target, it provides several advantages compared with the beam-scanning method, such as the reduced number of illuminations with the help of the compressed sensing algorithm [22]–[24] and robustness against background noises. [25].

The pseudo-random illumination patterns constitute the key factor in determining the performance of single-pixel imaging. They have been commonly generated by using bulky spatial light modulators (SLMs) based on digital micromirror devices (DMD) [11], [26] and liquid crystal on silicon (LCOS) [27]. Towards practical implementation of these systems, the authors have proposed and demonstrated the use of a compact and high-speed integrated optical phased array (OPA) in generating the illumination patterns [28], [29]. In addition, significant enhancement in spatial resolution was demonstrated by attaching a multimode fiber to the OPA chip [30], [31]. Large-scale OPAs have been developed on various integrated photonic platforms [32]–[34]. Owing to the recent advancement of silicon photonics and III-V heterogeneous integration technologies, ultra-compact single-chip OPA-based emitters with integrated laser sources and optical amplifiers are also feasible [35]. In addition, various techniques for monitoring and calibrating the optical field generated by an integrated OPA have been demonstrated to produce high-quality illumination patterns in real time [36]–[38].

One of the remaining issues of integrated OPAs is the complexity of the driver circuit. In particular, for the OPAs with reverse-biased electro-optic phase shifters, which are desirable for high-speed operation and low DC power consumption [32], [39], the requirement of high driving voltage to achieve 2π phase shift imposes a critical challenge when the number of phase shifters increases in the ranges of few hundreds to thousands. Therefore, it is important to alleviate the requirement of the driving conditions to reduce the complexity and the cost of the overall system.

In this paper, we investigate the phase shift requirement of OPA for single-pixel imaging and demonstrate, for the first time, that full 2π phase shifts are not mandatory to generate a set of illumination patterns with a sufficient degree of randomness required to reconstruct the image. Using a silicon photonic OPA chip with 128 carrier-depletion-based phase shifters, we experimentally confirm this property by retrieving an image under a maximum phase shift of only $\sim 1.5\pi$ without compromising the peak signal-to-noise ratio (PSNR) of the image. From a singular-value decomposition (SVD) analysis, we show that these results can be explained by the general dependence of the condition number of the illumination pattern matrix on the applied phase shift.

II. SINGLE-PIXEL IMAGING SCHEME

Fig. 1 shows the schematic of the single-pixel imaging using an OPA [29]. Input light is split into M waveguides via the cascaded stages of 1×2 multimode interference (MMI)
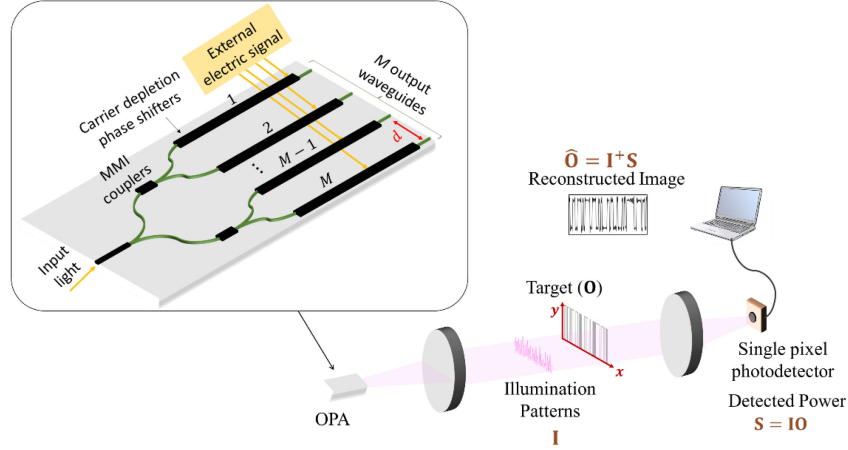
Fig. 1. Schematic of the single-pixel imaging using an OPA. The OPA generates the pseudo-random illuminations patterns (**I**) to sample the target (**O**). The transmitted power (**S**) is detected by the photodetector and finally the image (**Ô**) is reconstructed by the inverse reconstruction algorithm.

couplers. A random phase shift is applied at each waveguide, so that a speckle intensity pattern is generated at the far field of the chip output. By switching these electrical signals rapidly, we can generate a sequence of illumination patterns **I**, which is an $N \times P$ matrix representing the intensity at P pixels for N different illumination patterns. As these patterns interact with the target, the transmitted or reflected optical power is detected by a single-pixel photodetector. The detected signal for respective illumination patterns is described by an $N \times 1$ vector **S**. Finally, the image **Ô** is computationally obtained by

$$\hat{\mathbf{O}} = \mathbf{I}^+ \, \mathbf{S}, \qquad (1)$$

where $\mathbf{I}^+$ is the Moore-Penrose pseudo-inverse matrix of **I**.

In this work, for convenience, we consider a one-dimensional (1D) OPA as shown in Fig. 1, which generates 1D speckle patterns in x direction. We should note that two-dimensional (2D) imaging is possible by integrating grating couplers at the output waveguides and sweeping the wavelength of the light to steer the beam in another axis [35], [40].

III. EXPERIMENT

A. Silicon-Photonic OPA Chip With Carrier-Depletion Phase Shifters

Fig. 2 shows the silicon-photonic OPA chip with 128 carrier-depletion-based phase shifters used in this work. It was fabricated on a silicon-on-insulator (SOI) wafer with a Si layer of 220 nm and a buried oxide (BOX) layer of 2 μm in thickness. The waveguide width was set to 0.4 μm, whereas the output waveguide pitch was set to $d = 25$ μm.

We employed 3-mm-long phase shifters with interdigitated PN junctions with a pitch of 0.4 μm as shown in the inset of Fig. 2 [41]. By characterizing a test Mach-Zehnder interferometer (MZI) fabricated on the same chip, we confirmed that the 2π phase shift was obtained at -11V and +2.3V under the reverse and the forward biases, respectively.

The OPA chip was mounted on a chip carrier and all 128 phase shifters were driven randomly within the range from 0 to $\varphi_{\max}$. Due to the limitation of the maximum voltage that could be applied from our driver circuit, a combination of both the reverse
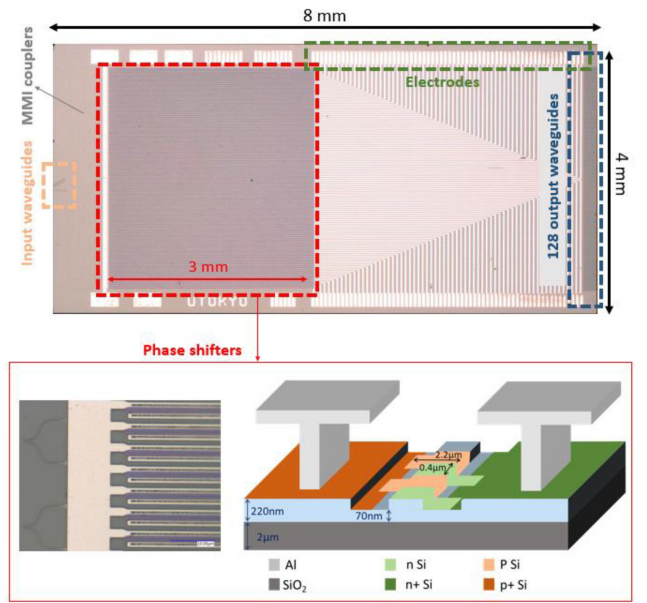

Fig. 2. Microscopic image of the silicon photonic OPA chip with 128 phase shifters used in the experiment. A zoomed image of the phase shifters and their cross section are shown in the inset.

and forward biases was employed in this work. For example, to achieve φ_{max} of 1.46π, we applied -4.0 V and +1.3 V to obtain around 0.86π and 0.60π phase shifts respectively, resulting in 1.46π in total. Operating in either mode would not affect the results of this study, however, it is to be noted that reverse-biased electro-optic phase shifters are generally preferred for faster operations and lower DC power consumption [32].

B. Experimental Setup

Fig. 3 shows the experimental setup of the single-pixel imaging using OPA. The input continuous-wave light with a wavelength of 1.55 μm was aligned to the transverse-electric (TE) mode and coupled into the OPA chip using a lensed fiber. Then, the light emitted from the chip was collected by the first lens (f_1) and sent through a 4f optical system (f_2 and f_3) so that the
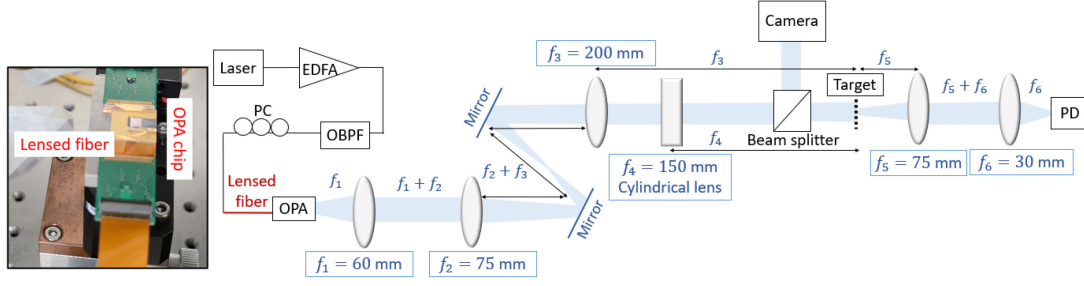
Fig. 3.   Experimental setup with a photograph of the mounted OPA chip as an inset. EDFA: erbium-doped fiber amplifier, OBPF: optical bandpass filter, PC: polarization controller, PD: photodetector.

far-field pattern (FFP) in the x direction was relayed to the target plane. In contrast, a cylindrical lens (f_4) was inserted to image the near-field pattern (NFP) in the y direction at the target plane. The focal length of each lens was chosen as described in Fig. 3, so that the free-spectral range (FSR) of the FFP in the x direction corresponded to 9.92 mm at the target. Two mirrors between the lenses f_2 and f_3 were inserted for convenience to facilitate the alignment by separating the system into two sections and align each of them separately. The light transmitted through the target was then focused by another 4f system and detected by a power meter (Agilent 81525A, InGaAs detector with a diameter of 5 mm). For convenience, a beam splitter was inserted to monitor the actual illumination pattern with an InGaAs infrared camera. In practice, the illumination patterns could be recorded first, followed by the actual single-pixel imaging procedure.

To compare the quality of the image under various conditions, we inserted a 1D slit pattern as a target with a minimum feature of 0.1 mm, corresponding to 90 features within one FSR. The image was reconstructed by using 1000 illumination patterns ($N = 1000$). For a quantitative evaluation, we use the peak signal-to-noise ratio (PSNR) of the retrieved image [29], which is defined as

$$\text{PSNR} = 10 \log \left(\frac{\max (O_i)^2}{\text{MSE}} \right) \text{[dB]}. \quad (2)$$

Here, MSE is the mean squared error, defined as $\text{MSE} = \frac{1}{P} \sum_i (O_i - \hat{O}_i)^2$, and O_i ($i = 1, \ldots, P$) is the actual image.

C. Results

Fig. 4(a) shows the experimentally retrieved images of the target as we vary the maximum phase shift $\varphi_{\max}$. The quality of the image improves monotonically with increasing $\varphi_{\max}$, as expected. Surprisingly, however, we can confirm that a clear image is obtained already at $\varphi_{\max} = 1.46\pi$ and its quality is comparable to that at $\varphi_{\max} = 1.92\pi$. Similar trend is also observed from the numerical results as shown in Fig. 4(b), where we assume a detector noise level of -10 dB in simulation to emulate the actual experimental case.

For quantitative comparison, Fig. 4(c) shows the PSNR of the retrieved image as a function of $\varphi_{\max}$. We can confirm an excellent agreement between the experimental and numerical results. Once again, we can see that the PSNR increases monotonically with $\varphi_{\max}$ but converges to a maximal value at around $\varphi_{\max} = 1.5\pi$.
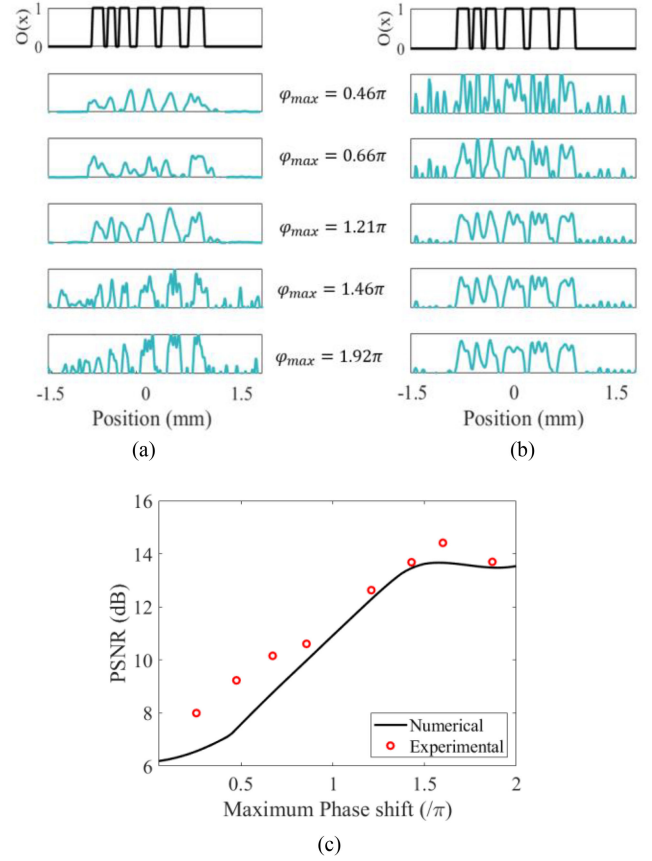

Fig. 4.   (a) Experimental and (b) numerical results of the reconstructed image $\hat{O}(x)$ (blue) for various values of the maximum phase shift $\varphi_{\max}$. The actual target $O(x)$ is plotted in black. (c) PSNR of the reconstructed image as a function of $\varphi_{\max}$ for the experimental (red dots) and numerical (black solid curve) results.

IV. DISCUSSIONS

The results shown in Fig. 4 imply that 2π phase shifts at the OPA are not necessarily required, and that $\sim 1.5\pi$ phase shifts are sufficient to generate the pseudo-random illumination patterns required for the single-pixel imaging. To evaluate the degree of randomness of the illumination patterns matrix, we employ the condition number, which is defined as [42]–[44]

$$\kappa (\mathbf{I}) = \frac{\sigma_{max}}{\sigma_{min}}, \quad (3)$$

where σ_{max} and σ_{min} are the maximum and minimum singular values of the matrix $\mathbf{I}$, respectively. When the condition number
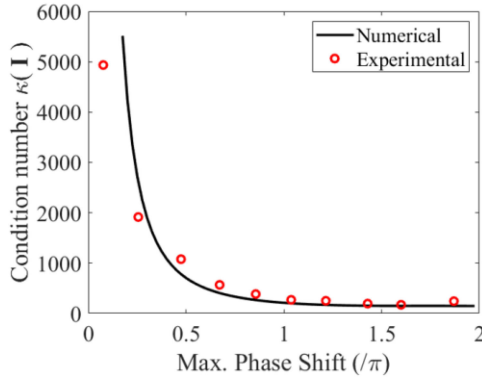
Fig. 5. Condition number of the illumination patterns matrix as a function of the maximum phase shift $\varphi_{\max}$, obtained numerically (black solid curve) and experimentally (red dots).
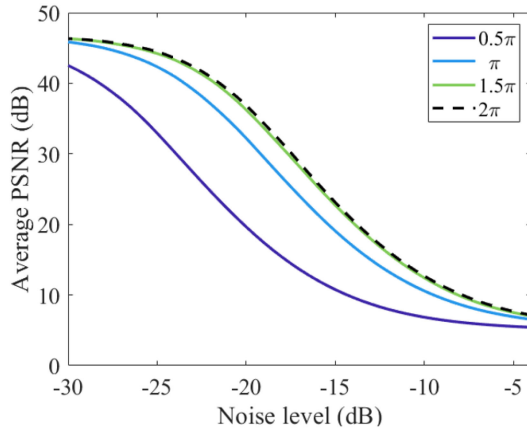

Fig. 6. Average PSNR for 10 random targets generated in simulation as a function of the detector noise level for different values of the maximum phase shifts $\varphi_{\max}$.

is large, the matrix is ill-conditioned, or in other words, the randomness of the illumination patterns is weak.

Fig. 5 shows the condition number of the illumination matrix **I**, which is obtained both experimentally and numerically, as a function of $\varphi_{\max}$. While the condition number reduces as $\varphi_{\max}$ increases, we can see that it approaches the steady value for $\varphi_{\max} > \pi$. This trend is consistent with Fig. 4 and reveals the fact that a sufficient randomness of the illumination patterns can be attained at a significantly smaller phase shift.

To confirm that these results are valid regardless of the detector noise level, we also simulate the single-pixel imaging performance at different noise levels. Fig. 6 shows the average PSNR of the retrieved image for 10 different targets, each generated randomly with the minimum feature corresponding to the actual experimental case. The noise level is defined as

$$\text{Noise level} = 10 \log \left(\frac{\mu_s}{\sigma_{noise}} \right) \text{ [dB]}, \qquad (4)$$

where μ_s is the average power detected at the single-pixel photodetector, and σ_{noise} is the standard deviation of the detector noise, which was assumed to be Gaussian.

From Fig. 6, we can observe that the dependence on the noise level starts to converge when $\varphi_{\max} > \pi$ and becomes almost identical at $\varphi_{\max} > 1.5\pi$. We can therefore conclude that the

maximum phase shift of OPA can be reduced to around 1.5π without sacrificing the imaging quality. These results have a significant impact particularly for an OPA with carrier-depletion-based phase shifters, which generally suffer from large driving voltage to induce 2π phase shifts.

V. CONCLUSION

We have demonstrated numerically and experimentally that by using a silicon OPA with 128 carrier-depletion-based phase shifters, clear imaging with 90 resolvable points was possible at a maximum phase shift of only $\sim 1.5\pi$. This trend was directly linked to the condition number of the illumination matrix, which indicates the randomness of the illumination patterns. It was therefore revealed that full 2π phase shifts are not mandatory to ensure the randomness of the illumination patterns required for single-pixel imaging. As a result, we could taper off the device requirement by reducing the applied voltages to the phase shifters without affecting the quality of the retrieved image. Such feature is in clear contrast to the beam-scanning method and is particularly attractive for a carrier-depletion-based OPA, which generally requires large voltages to attain 2π phase shifts. This work would therefore pave the way to performing high-speed OPA-based imaging with a minimum device requirement.

REFERENCES

[1] M. -J. Sun et al., "Single-pixel three-dimensional imaging with time-based depth resolution," *Nature Commun.*, vol. 7, no. 1, Jul. 2016, Art. no. 12010.
[2] M. J. Padgett and R. Boyd, "An introduction to ghost imaging: Quantum and classical," *Phil. Trans. R. Soc. A*, vol. 375, no. 2099, Aug. 2017, Art. no. 20160233.
[3] Y. Bromberg, O. Katz, and Y. Silberberg, "Ghost imaging with a single detector," *Phys. Rev. A*, vol. 79, no. 5, May 2009, Art. no. 053840.
[4] M. -J. Sun and J. -M. Zhang, "Single-pixel imaging and its application in three-dimensional reconstruction: A brief review," *Sensors*, vol. 19, no. 3, pp. 732–745, 2019.
[5] Z. Zhang and J. Zhong, "Three-dimensional single-pixel imaging with far fewer measurements than effective image pixels," *Opt. Lett.*, vol. 41, no. 11, pp. 2497–2500, 2016.
[6] E. Salvador-Balaguer, P. Latorre-Carmona; C. Chabert, F. Pla, J. Lancis, and E. E. Tajahuerce, "Low-cost single-pixel 3D imaging by using an LED array," *Opt. Exp.*, vol. 26, no. 12, pp. 15623–15631, 2018.
[7] G. M. Gibson, S. D. Johnson, and M. J. Padgett, "Single-pixel imaging 12 years on: A review," *Opt. Exp.*, vol. 28, no. 19, pp. 28190–28208, 2020.
[8] J. H. Shapiro, "Computational ghost imaging," *Phys. Rev. A*, vol. 78, no. 6, Dec. 2008, Art. no. 061802.
[9] M. P. Edgar, G. M. Gibson, and M. J. Padgett, "Principles and prospects for single-pixel imaging," *Nature Photon.*, vol. 13, no. 1, pp. 13–20, Jan. 2019.
[10] S. Welsh, M. Edgar, R. Bowman, P. Jonathan, B. Sun, and M. J. Padgett, "Fast full-color computational imaging with single-pixel detectors," *Opt. Exp.*, vol. 21, no. 20, pp. 23068–23074, Oct. 2013.
[11] N. Radwell, K. J. Mitchell, G. M. Gibson, M. P. Edgar, R. Bowman, and M. J. Padgett, "Single-pixel infrared and visible microscope," *Optica*, vol. 1, no. 5, pp. 285–289, Oct. 2014.
[12] W. Gong, C. Zhao, H. Yu, M. Chen, W. Xu, and S. Han, "Three-dimensional ghost imaging lidar via sparsity constraint," *Sci. Rep.*, vol. 6, May 2016, Art. no. 26133.
[13] S. Johnson, N. Radwell, M. Edgar, C. Higham, R. Murray-Smith, and M. Padgett, "Single-pixel LIDAR with deep learning optimised sampling," in *Proc. Conf. Lasers Electro-Opt.*, 2020, pp. 1–2.
[14] S. Ma et al., "Ghost imaging LiDAR via sparsity constraints using push-broom scanning," *Opt. Exp.*, vol. 27, no. 9, pp. 13219–13228, Apr. 2019.
[15] B. Lochocki et al., "Single pixel camera ophthalmoscope," *Optica*, vol. 3, no. 10, pp. 1056–1059, Sep. 2016.
[16] R. I. Stantchev et al., "Noninvasive, near-field terahertz imaging of hidden objects using a single-pixel detector," *Sci. Adv.*, vol. 2, no. 6, Jun. 2016, Art. no. e1600190.

[17] D. Shrekenhamer, C. M. Watts, and W. J. Padilla, "Terahertz single-pixel imaging with an optically controlled dynamic spatial light modulator," *Opt. Exp.*, vol. 21, no. 10, pp. 12507–12518, May 2013.

[18] G. A. Howland, D. J. Lum, M. R. Ware, and J. C. Howell, "Photon counting compressive depth mapping," *Opt. Exp.*, vol. 21, no. 20, pp. 23822–23837, Oct. 2013.

[19] B. Sun, M. P. Edgar, R. Bowman, L. E. Vittert, S. Welsh, and A. Bowman, "3D computational imaging with single-pixel detectors," *Science*, vol. 340, no. 6134, pp. 844–847, May 2013.

[20] M. Wang, M. -J. Sun, and C. Huang, "Single-pixel 3D reconstruction via a high-speed LED array," *J. Phys. Photon.*, vol. 2, no. 2, Apr. 2020, Art. no. 025006.

[21] S. Ota *et al.*, "Ghost cytometry," *Science*, vol. 360, no. 6394, pp. 1246–1251, Jun. 2018.

[22] T. Jia, D. Chen, J. Wang, and D. Xu, "Single-pixel color imaging method with a compressive sensing measurement matrix," *Appl. Sci.*, vol. 8, no. 8, Aug. 2018, Art. no. 1293.

[23] M. F. Duarte *et al.*, "Single-pixel imaging via compressive sampling," *IEEE Signal Process. Mag.*, vol. 25, no. 2, pp. 83–91, Mar. 2008.

[24] O. Katz, Y. Bromberg, and Y. Silberberg, "Compressive ghost imaging," *Appl. Phys. Lett.*, vol. 95, no. 13, Sep. 2009, Art. no. 131110.

[25] Z. Yang, W. X. Zhang, M. C. Zhang, D. Ruan, and J. L. Li, "Instant ghost imaging: Improving robustness for ghost imaging subject to optical background noise," *OSA Continuum*, vol. 3, no. 2, pp. 391–400, Feb. 2020.

[26] M. P. Edgar, G. M. Gibson, R. W. Bowman, B. Sun, N. Radwell, and K. J. Mitchell, "Simultaneous real-time visible and infrared video with single-pixel detectors," *Sci. Rep.*, vol. 5, no. 1, May 2015, Art. no. 10669.

[27] P. Clemente, V. Durán, V. Torres-Company, E. Tajahuerce, and J. Lancis, "Optical encryption based on computational ghost imaging," *Opt. Lett.*, vol. 35, no. 14, pp. 2391–2393, Jul. 2010.

[28] K. Komatsu, Y. Ozeki, Y. Nakano, and T. Tanemura, "Ghost imaging using integrated optical phased array," in *Proc. Opt. Fiber Commun. Conf. Exhib.*, 2017, pp. 1–3.

[29] Y. Kohno, K. Komatsu, R. Tang, Y. Ozeki, Y. Nakano, and T. Tanemura, "Ghost imaging using a large-scale silicon photonic phased array chip," *Opt. Exp.*, vol. 27, no. 3, pp. 3817–3823, Feb. 2019.

[30] T. Fukui, Y. Kohno, R. Tang, Y. Nakano, and T. Tanemura, "Single-pixel imaging using multimode fiber and silicon photonic phased array," *J. Lightw. Technol.*, vol. 39, no. 3, pp. 839–844, Feb. 2021.

[31] T. Fukui, Y. Nakano, and T. Tanemura, "Resolution limit of single-pixel speckle imaging using multimode fiber and optical phased array," *J. Opt. Soc. Amer. B*, vol. 38, no. 2, pp. 379–386, Feb. 2021.

[32] C. V. Poulton *et al.*, "Long-range LiDAR and free-space data communication with high-performance optical phased arrays," *IEEE J. Sel. Top. Quantum Electron.*, vol. 25, no. 5, Sept./Oct. 2019, Art. no. 7700108.

[33] S. Chung, H. Abediasl, and H. Hashemi, "A monolithically integrated large-scale optical phased array in silicon-on-insulator CMOS," *IEEE J. Solid-State Circ.*, vol. 53, no. 1, pp. 275–296, Jan. 2018.

[34] K. Komatsu, Y. Kohno, Y. Nakano, and T. Tanemura, "Large-scale monolithic inp-based optical phased array," *IEEE Photon. Technol. Lett.*, vol. 33, no. 20, pp. 1123–1126, Oct. 2021.

[35] J. C. Hulme *et al.*, "Fully integrated hybrid silicon two dimensional beam scanner," *Opt. Exp.*, vol. 23, no. 5, pp. 5861–5874, Mar. 2015.

[36] J. Shim *et al.*, "On-chip monitoring of far-field patterns using a planar diffractor in a silicon-based optical phased array," *Opt. Lett.*, vol. 45, no. 21, pp. 6058–6061, Nov. 2020.

[37] J. Ø. Kjellman *et al.*, "Silicon photonic phase interrogators for on-chip calibration of optical phased arrays," in *Proc. SPIE*, 2020, Art. no. 112830X.

[38] L. J. Li, W. Chen, X. Y. Zhao, and M. -J. Sun, "Fast optical phased array calibration technique for random phase modulation LiDAR," *IEEE Photon. J.*, vol. 11, no. 1, Feb. 2019, Art. no. 6900410.

[39] G. Kang *et al.*, "Silicon-based optical phased array using electro-optic p-i-n phase shifters," *IEEE Photon. Technol. Lett.*, vol. 31, no. 21, pp. 1685–1688, Nov. 2019.

[40] D. N. Hutchison *et al.*, "High-resolution aliasing-free optical beam steering," *Optica*, vol. 3, no. 8, pp. 887–890, Aug. 2016.

[41] H. Yu *et al.*, "Performance tradeoff between lateral and interdigitated doping patterns for high speed carrier-depletion based silicon modulators," *Opt. Exp.*, vol. 20, no. 12, pp. 12926–12938, Jun. 2012.

[42] S. Emara, T. Fukui, K. Komatsu, Y. Kohno, T. Tanemura, and Y. Nakano, "Optimization based on the condition number of the speckle patterns in single-pixel imaging using optical phased arrays," *Japanese J. Appl. Phys.*, vol. 60, no. 7, Jul. 2021, Art. no. 072006.

[43] G. Golub and W. Kahan, "Calculating the singular values and pseudo-inverse of a matrix," *J. Soc. Ind. Appl. Math. Ser. B Numer. Anal.*, vol. 2, no. 2, pp. 205–224, 1965.

[44] A. K. Cline, C. B. Moler, G. W. Stewart, and J. H. Wilkinson, "An estimate for the condition number of a matrix," *J. Soc. Ind. Appl. Math. Numer. Anal.*, vol. 16, no. 2, pp. 368–375, 1979.